PERGAMON

International Journal of Solids and Structures 39 (2002) 3159–3173

INTERNATIONAL JOURNAL OF SOLIDS and STRUCTURES

www.elsevier.com/locate/ijsolstr

Determination of sensor positions for predictive maintenance of revolving machines

F. Bogard, K. Debray, Y.Q. Guo *

Laboratory GMMS (Mechanics, Materials & Structures), University of Reims Champagne-Ardenne, Rue des Crayères BP 1035, 51687 Reims Cedex 2, France

Received 23 July 2001; received in revised form 1 November 2001; accepted 9 January 2002

Abstract

The monitoring by measurement and analysis of vibration is largely used to detect the defects in revolving machines. The determination of the best sensor positions is one of the main research goals in the field of predictive maintenance. This paper proposes a numerical methodology based on a finite element model and a spectral analysis in order to find optimum sensor positions. The bearing is a key component for the vibration propagation from the moving parts to static ones. An analytical bearing model and its numerical implementation in a finite element code are presented. The tangent stiffness matrix of the bearing element is obtained by the Newton–Raphson method and then used for the modal and spectral analyses. Several techniques are used to find the most sensitive zones to common defects. The proposed numerical approach correlate well with the experimental results. The numerical modeling of a grinder shows the interests in industrial applications.

Keywords: Ball bearing; Finite element of bearing; Modal analysis; Experimental validation; Conditional maintenance

1. Introduction

The follow-up of the damage of some parts in a rotating machine by vibration analysis is a widely used technique in the predictive maintenance. The purpose of this type of maintenance, advantageous to the curative and periodic maintenance, is to carry out an intervention on a part just before its mechanical failure (AFNOR, 1995). This requires the monitoring and analysis of the evolution of vibration spectrums at one or several points on the machine in order to detect the characteristic peaks of common defects (Max, 1987). For the vibration follow-up of the bearings, it is possible to calculate in advance the frequencies of ring or ball defects according to the bearing geometry and its rotating speed (Morel, 1992). In most cases, the ideal measurement points are situated near the parts to be followed up, but the size of some machines and the accessibility to certain areas makes it difficult, even impossible, to take the measurements in these places.

* Corresponding author. Tel.: +33-3-2691-3158; fax: +33-3-2691-3075.
E-mail address: yq.guo@univ-reims.fr (Y.Q. Guo).

0020-7683/02/$ - see front matter
PII: S0020-7683(02)00117-8

Although the reliability of defect detecting in the predictive maintenance has made enormous improvements, mainly due to the computer treatment of vibratory signals, it is nevertheless greatly dependant on the quality of signal analysis and positioning of sensors.

This study proposes a methodology based on a numerical approach in order to find an optimum sensor implementation on a revolving machine. The numerical modeling allows to determine the number and the location of measurement points. Particular consideration is given to a common component on revolving machines: the bearing which is the only material link between the moving part and the immobile part in the vibration transmission.

Firstly an analytical model for the rolling ball bearing is presented. The relations between the displacements (rotations) and the forces (torques) are obtained by using the cinematic relations and the Hertz contact theory. The formulation of the bearing element and its implementation in a finite element software are described. The model and the spectral analyses are used to determine the most sensitive zones for given defects. This numerical methodology is validated with an experimental academic example. Moreover, the comparison between the numerical and experimental results of an industrial grinder shows the interest of this application in the sensor monitoring setting for the predictive maintenance.

2. Bearing modeling and its numerical implementation

The numerical modeling of an elementary cell of a revolving machine (the whole shaft-bearing-housing) in detail is very tedious and complicated because of the contact treatment. An analytical model is presented here to obtain an equivalent stiffness of the ball bearing and then its finite element implementation in order to carry out the vibration analysis.

2.1. Definition of the bearing stiffness matrix

Numerous problems are involved in analytical models of the bearing because of its strongly non-linear elastic behavior. This non-linearity is due to the Hertzien contact and the clearance between the rolling elements and the rings. Moreover, the load intensity, supported individually by each ball, depends on the internal geometry of the bearing as well as the type of the applied load.

Many publications have been presented on the evaluation of the life duration of the ball and roller bearings in function of the applied excitations (Palmgren, 1959; Jones, 1960; Harris, 1991).

Several researchers have also studied the equivalent stiffness of bearings (Lim and Singh, 1990; Demul et al., 1989). They proposed an analytical model and a stiffness matrix with 5 degrees of freedom on the inner ring (3 translations and 2 rotations; the rotation around the shaft is free). The proposed matrix included coupling of the bending movements between the shaft and housing and take into account the effects of the centrifugal forces and the gyroscopic moments.

For the studied case, the effects of the centrifugal forces and gyroscopic moments have only a little influence on the coupling coefficients because of the low angular speed of the shaft. Our approach is based on the above works but without considering these effects. The analytical bearing model consists in determining the relations between the displacements (rotations) and the applied forces (torques) at the center O of the bearing.

The geometry of a ball bearing with oblique contact are presented in Fig. 1 where a_i and a_e are the curvature centers of the inner and outer rings, A_0 and A_j are the distances between these two centers before and after loading, δ_{rj} and δ_{zj} are the effective displacements in the radial and axial directions for the ball number j, δ_i and β_i, are the displacement and rotation at the center O. Fig. 1 also shows the external forces $\{F\}$ acting on the gravity center of the radial ball bearing. The components of this force in the global cartesian system (XYZ) are:

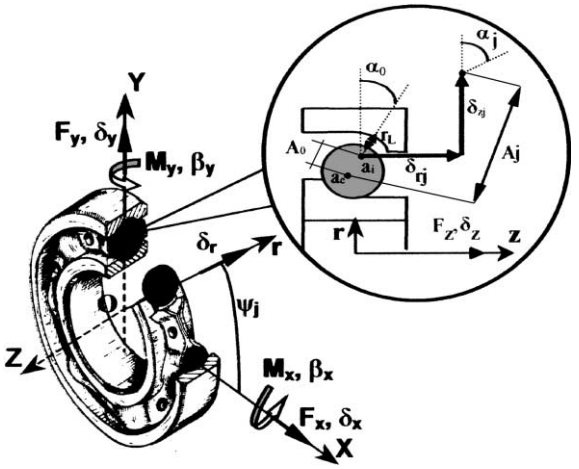

Fig. 1. Geometry and cinematic relations of a ball bearing with oblique contact.

$$\{F\} = \langle F_X \quad F_Y \quad F_Z \quad M_X \quad M_Y \rangle^{\mathrm{T}} \tag{1}$$

this external force vector depends on the assembly of the shaft-bearing and can be obtained from the static equilibrium of the system. The external forces $\{F\}$ must be in balance with the internal forces $\{Q\}$ resulting from the superposition of the forces of all balls on the inner ring:

$$\{F\} + \{Q\} = \{0\} \tag{2}$$

The force Q_j applied on the jth ball, can be written as follows according to the Hertz theory:

$$Q_j = K\delta_j^m \quad \text{with} \begin{cases} \delta_j = A_j - A_0, & \forall A_j > A_0 \\ \delta_j = 0, & \forall A_j < A_0 \end{cases} \tag{3}$$

where K is the stiffness constant which depends on the nature and the geometry of the components in contact, the exponent m is equal to 1.5 in the case of a ball bearing (Harris, 1991).

A geometric study on the displacement of the point M and the curvature center of the inner ring, shows that the distance A_j is relative to several geometric dimensions of the bearing, but also to the displacement $\vec{u}_M$. The contact force calculated for each ball can be cumulated and then projected in the reference (rtz) in order to obtain the contact force components:

$$\vec{u}_M = u_r\vec{r} + u_z\vec{z} \quad \text{and} \quad \{Q\}_{rtz} = \langle Q_r \quad Q_z \quad T \rangle^{\mathrm{T}} \tag{4}$$

where Q_r and Q_z are the components of the contact forces in the r and z directions, T is the torque around the $\vec{t}$ axis. By choosing the M point at the curvature center, the torque T is always equal to zero. The resultant forces in the global reference (XYZ) can be easily obtained with the transformation matrix $[R_\phi]$:

$$\{Q\} = \left[R_\phi\right]^{\mathrm{T}}\{Q\}_{rtz} \quad \text{with } [R_\phi] = \begin{bmatrix} \cos\phi & \sin\phi & 0 & -z_m\sin\phi & z_m\cos\phi \\ 0 & 0 & 1 & r_m\sin\phi & -r_m\cos\phi \\ 0 & 0 & 0 & -\sin\phi & \cos\phi \end{bmatrix} \tag{5}$$

where z_m and r_m are the components of the curvature centre in the (rtz) reference.

This matrix allows to express the displacement $\vec{u}_M$ of the curvature centre M in the (rtz) reference, according to the displacements $\vec{\delta}$ of the point O in the (XYZ) reference:

$$\{u_M\}_{rtz} = \left[R_\phi\right]\{\delta\} \quad \text{with } \{\delta\} = \langle \delta_X \quad \delta_Y \quad \delta_Z \quad \beta_X \quad \beta_Y \rangle^{\mathrm{T}} \tag{6}$$

where δ_i and β_i are the translation and rotation components of the point O expressed in the (XYZ) reference.

Eqs. (2) and (5) give the following non linear system:

$$\{R\} = \{F\} + \sum_{j=1}^{n} \left[R_\phi\right]_j^{\mathrm{T}} \{Q\}_j = 0 \tag{7}$$

where $\{R\}$ is the residual force vector, n the number of balls. The Newton–Raphson method is used to solve the above system and obtain the tangent stiffness matrix at the given load level:

$$[K_T]\{\Delta\delta\} = \{R\} \quad \text{and} \quad \{\delta^{i+1}\} = \{\delta^i\} + \{\Delta\delta\} \tag{8}$$

with

$$[K_T] = -\left[\frac{\partial\{R\}}{\partial\langle\delta\rangle}\right] = -\sum_{j=1}^{n} \left[R_\phi\right]_j^{\mathrm{T}} \left[\frac{\partial\{Q\}_j}{\partial\langle u_M\rangle}\right] \left[\frac{\partial\{u_M\}}{\partial\langle\delta\rangle}\right] \tag{9}$$

$$[K_T] = -\sum_{j=1}^{n} \left[R_\phi\right]_j^{\mathrm{T}} \left[K'\right]_j \left[R_\phi\right]_j \tag{10}$$

where $\{\Delta\delta\}$ is the displacement increment, $[K']$ is the contact stiffness matrix (3×3) defined in the (rtz) reference, $[K_T]$ is the tangent stiffness matrix (5×5) defined in the global (XYZ) reference.

2.2. Numerical implantation of the bearing element

The calculations were carried out using the ABAQUS® code. The ball bearing model was implemented in the ABAQUS code by developing a 'bearing' element with two nodes and five dof per node using the above tangent stiffness matrix. The objective is to replace the bearings by some bearing elements. These links ensure, with the help of the tangent stiffness matrix, the vibration transmission from the shaft to the housing. The outer ring of the bearing is very rigid and fixed on the housing bore. This ring is connected to the shaft by using four bearing elements (Fig. 2). The stiffness matrix of each element is a quarter of the global stiffness matrix defined previously:

$$[K_T]_i = \tfrac{1}{4}[K_T] \quad (\forall i = 1, 2, 3, 4) \tag{11}$$

The number of connections have been chosen according to several tests using 3, 4, 6, 12 and 16 bearing elements. The comparison shows that four connections are adequate for studied vibration system.

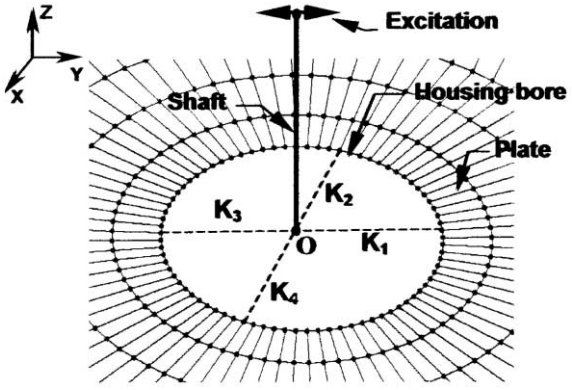

Fig. 2. Connection between the shaft and the housing with 'bearing elements'.

3. Dynamic analysis to find optimum sensors placements

The determination of the optimum sensor positions needs a dynamic analysis and an exploitation of the obtained eigenvectors or dynamic response vectors.

3.1. Excitation forces

In a revolving machine, the most sensitive organs are often the bearings. The emergence of different defects on these bearings involves different dynamic excitations which allows to characterize the types of defects (Appendix A). The usual defects are of course the chipping defects on the inner ring, outer ring or on the balls.

An excitation can be decomposed in three components in the $(X\,Y\,Z)$ reference according to the contact angle α and the angular position φ_d of the defect:

$$\begin{cases} F_X = F_l \cos(\alpha)\cos(\varphi_d) \\ F_Y = F_l \cos(\alpha)\sin(\varphi_d) \\ F_Z = F_l \sin(\alpha) \end{cases} \tag{12}$$

For a defect on the fixed outer ring, the direction of the force F_l and the angle φ_d due to the defect do not change, but if the defect is situated on the inner ring or on a ball, then φ_d is time dependent. In this paper, only the defects on the outer ring giving a constant angle φ_d are studied.

The excitations generated by defects are periodic signals whose shapes can be assumed as rectangular, triangular or sinusoidal pulses (Fig. 3). The pulse width ΔT depends on the defect size and the relative speed between rolling elements (Tandon and Choudury, 1997). Three pulse width are considered: 10%, 30% and 50% of the period T. With these assumptions, an excitation can be written in Fourier series (Eq. (15)). For each of these excitation signals, Fourier coefficient F_0 and F_k are developed in Appendix B. Here we take 20 terms in the series ($N_f = 20$). The final response is the sum of the responses excited by every pulsation $k\omega_n$.

3.2. Dynamic analysis in the frequency domain

A standard dynamic problem can be described by the following system:

$$[M]\{\ddot{q}(t)\} + [C]\{\dot{q}(t)\} + [K]\{q(t)\} = \{F(t)\} \tag{13}$$

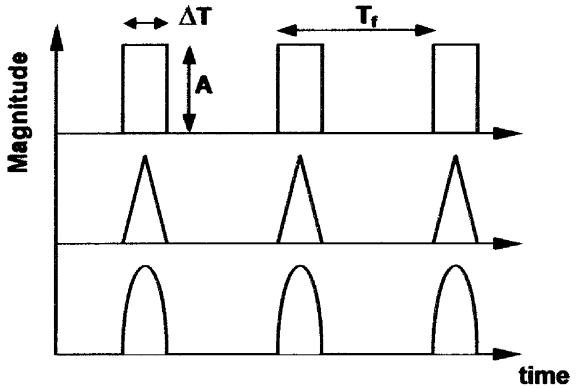

Fig. 3. Pulse shapes of defect excitations.

where $[M]$ is the symmetric mass matrix, $[C]$ the damping matrix, $[K]$ the stiffness matrix, $\{q\}$ the displacement vector, the excitation vector $\{F(t)\}$ is a periodic function, but is not necessarily an harmonic function.

The first step consists in solving the eigenvalue problem by a classical vibration analysis. This problem of free vibration is defined as follows:

$$[M]\{\ddot{q}\} + [K]\{q\} = 0 \tag{14}$$

By setting $\{q(t)\} = \{q\}e^{i\omega t}$ with the amplitude vector $\{q\}$ independent of the time, the eigenvalue problem is solved by the method of subspace iteration to obtain the eigenvalue ω, the eigenvector $\{\phi\}$ and the modal matrix $[\Phi] = [\{\phi_1\} \quad \cdots \quad \{\phi_n\} \quad \cdots]$.

In the second step, a spectral analysis is carried out in the frequency domain. The excitation vector is decomposed in Fourier series, taking into account the parity of the excitation signal:

$$\{F(t)\} = \{F_0\} + \sum_{n=1}^{n=+\infty} \{F_n\} \cos(\omega_n t) \tag{15}$$

with

$$\{F_n\} = \frac{2}{T} \int_{-\frac{T}{2}}^{+\frac{T}{2}} \{F(t)\} \cos(\omega_n t) \mathrm{d}t; \quad \omega_n = n\omega_f; \quad \omega_f = \frac{2\pi}{T_f} \tag{16}$$

where T_f is the period of a defect excitation.

The study is restricted to permanent response in steady states. Every harmonic excitation in the Fourier series gives an harmonic response which can be express in the frequency domain using a Fourier transform. Using the modal superposition method, we obtain the following dynamic response:

$$\{q(\omega_f)\} = \sum_{n=1}^{N_f} \sum_{j=1}^{\text{nb modes}} \{\phi_j\} H_j \{\phi_j\}^{\mathrm{T}} \{F_n\} \tag{17}$$

with the frequency response function:

$$H_j(\omega_f) = \frac{1}{\omega_f^2 M_j + i\omega_f C_j + K_j} \tag{18}$$

where M_j, C_j, K_j are jth components of the diagonal mass, damping and stiffness matrices. To facilitate the resolution the modal damping C_j is defined as the function of the damping ratio ξ_j in the mode j characterized by the pulsation ω_j:

$$C_j = 2\xi_j \omega_j \tag{19}$$

3.3. Two methods for defect detection

Two methods are presented to determine the optimum sensor positions for the defect detection.

3.3.1. Mode shape summation method

This method is based on the summation of the first p normalized natural modes obtained by the eigenvalue computation:

$$\{\phi_{\text{MSSM}}\} = \sum_{i=1}^{p} \{\phi_i\} \tag{20}$$

The maximal absolute value in the vector $\{\phi_{\mathrm{MSSM}}\}$ indicates the maximal vibration amplitude and the corresponding degree of freedom, so the sensor positions can be easily obtained. This method was developed to determine the measurement locations for an experiment modal test (De Clerck and Avitabile, 1996). It does not consider the contribution percentage of each mode neither the influence of the excitation defects; the choice of the frequency interval and the number of modes is a difficult task. Its application in this study is for the tentative identification for the measurement locations of defect detection. However, this is beyond the intended use of MSSM.

3.3.2. Defect response method

This method is based on the spectral analysis in the frequency domain. The defect excitations are assumed periodic with the periods T_{or}, T_{ir}, T_{ball} and T_{cage} relative to the outer ring, inner ring, the balls and to the cage. The obtained defect response vectors can be used to find the optimum sensor positions. In practice, the sensors allow to detect only the vibration perpendicular to the installation surface, so these response vectors should be projected in the normal directions of surfaces; only the absolute values of these projections are used to determine the sensor positions.

This method is more rigorous than the mode shape summation method (MSSM), but numerous defect excitations (different directions and frequencies) will give many choices.

One possibility to reduce the number of choices is to sum these response vectors as follows:

$$\{q_{\mathrm{RESP}}\} = \sum_{d=1}^{\mathrm{Nb\ freq\ defect}} \{q_{\mathrm{d}}\} \tag{21}$$

This technique is very simple to implement, but it mixes the contributions of all defects without considering weighting coefficients which are not easy to choose.

4. Numerical and experimental results on a bearing plate mount

4.1. Description of the experimental device

An experimental device (Fig. 4) is made to produce the dynamic effects on the bearing and housing in a revolving machine (Bogard, 2000). This device is an elementary cell composed of a shaft (145 mm, ∅25 mm) in steel alloy XC38. The shaft is fitted on two identical ball bearings SNR 6205, separated by a distance of 42 mm. The upper bearing is fitted on an aluminum alloy plate 2024 ($5.96 \times 400 \times 600\ \mathrm{mm}^3$), representing the housing. This plate is fixed on its perimeter by eight massive bars in steel XC38 ($46 \times 46\ \mathrm{mm}^2$),

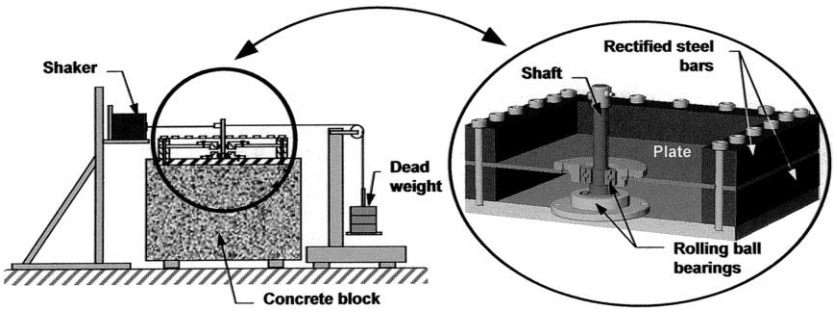

Fig. 4. Experimental mount of the elementary cell.

which are fixed to a concrete support with 38 bolts in order to obtain embedding boundary conditions. The lower bearing is directly fitted on a steel plate embedded in the concrete block.

The free extremity of the shaft is subjected to a radial pre-load of 193 N in the *Oy* direction obtained with a dead weight. This pre-load eliminates the shocks due to the internal clearance of the bearing. It can be observed that the rotation speed of the shaft has no influence on the bearing stiffness in the considered speed range; the difference of the stiffness between the static and the dynamic cases is neglected (Kraus et al., 1987). A white noise signal is applied on the free extremity of the shaft in the *Oy* direction by a shaker. This kind of signal allows to excite the system in a realistic way in order to validate some assumptions in the present numerical model.

4.2. Identification of experimental modes

The experimental measurements frequency response functions (FRF) are exploited by using a modal analysis software, Matlab Toolbox® (SDT, 1999). The purpose is to identify the excited frequencies and modal shapes of the system: the measurements, taken on 25 points on the structures, are interpolated by the software to determine the excited frequencies; a graphic interface allows to show the vibration modes and to compare them with the numerical modes.

4.3. Numerical modeling and experimental validation

Firstly the dynamic behaviors of the elementary cell are studied without considering the bearing. The aluminium plate is discretized with the four node plate element and the shaft with the two node 3D beam element (Timoshenko). The rigorous embedding boundary conditions are very difficult to obtain experimentally, so in the present numerical modeling, pseudo-embedding conditions are determined by a parameter identification. The FRF measured frequencies and the calculated ones by the FE method in the range of 0–2 kHz are in a quite good agreement. Some of the peaks are the result of local modes of the structure that are not of interest or concern for the evaluation under consideration. But, for the first ten modes, the average error is lower than 7%, so the parameter choices in the modeling of the housing–bearing unit are considered a reasonable choice.

Then, FRF of the device are computed by using the bearing element and imposing a white noise on the free extremity of the shaft. The experimental acquisition is achieved with a multi-channel card in the frequency range of 0–2 kHz. The comparison between experimental and numerical results is carried out by superposing the numerical results and FRF measurements evaluated on a same point and in the normal direction Z.

The above FRF comparison is not always sufficient to validate the numerical model. A modal analysis, realized with the Matlab Toolbox software, allows to identify with certitude the frequencies and associated vibration modes, then to compare them with calculated modes. A fairly good correlation can be observed between the experimental and numerical modal shapes (Fig. 5), which confirms the present bearing model and the corresponding finite element.

4.4. Numerical application of the two methods for defect detection

The two methods MSSM and defect response method (DRM) are applied to the elementary cell to study their influence on the defect detection using an excitation on the outer ring of the ball bearing. The comparison of the amplitude isovalues obtained by the both methods shows:

- The MSSM gives incoherent results with respect to the symmetric geometry of the elementary cell (Fig. 6a). In fact, the summation of the symmetric and anti-symmetric modes gives a non symmetric distribu-

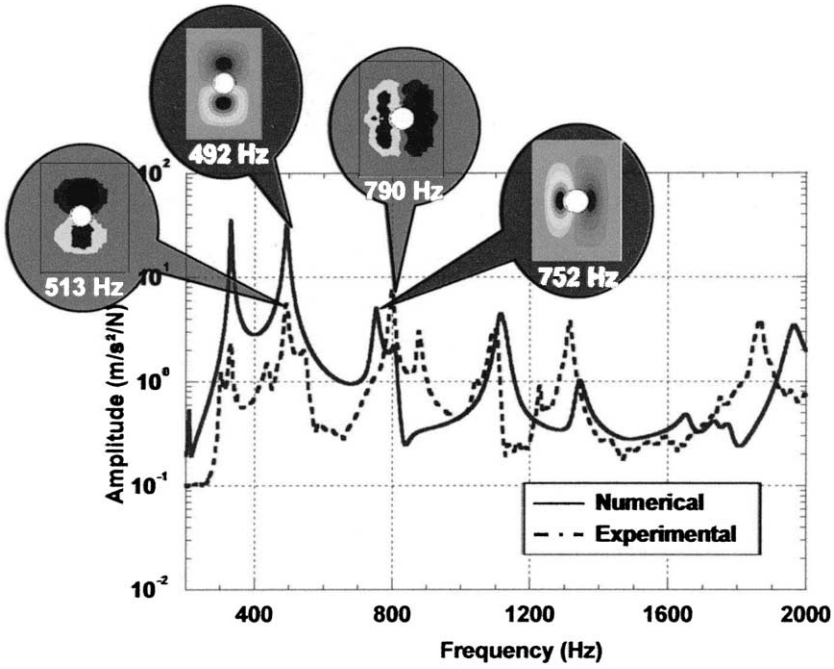

Fig. 5. Experimental validation of the spectral response.

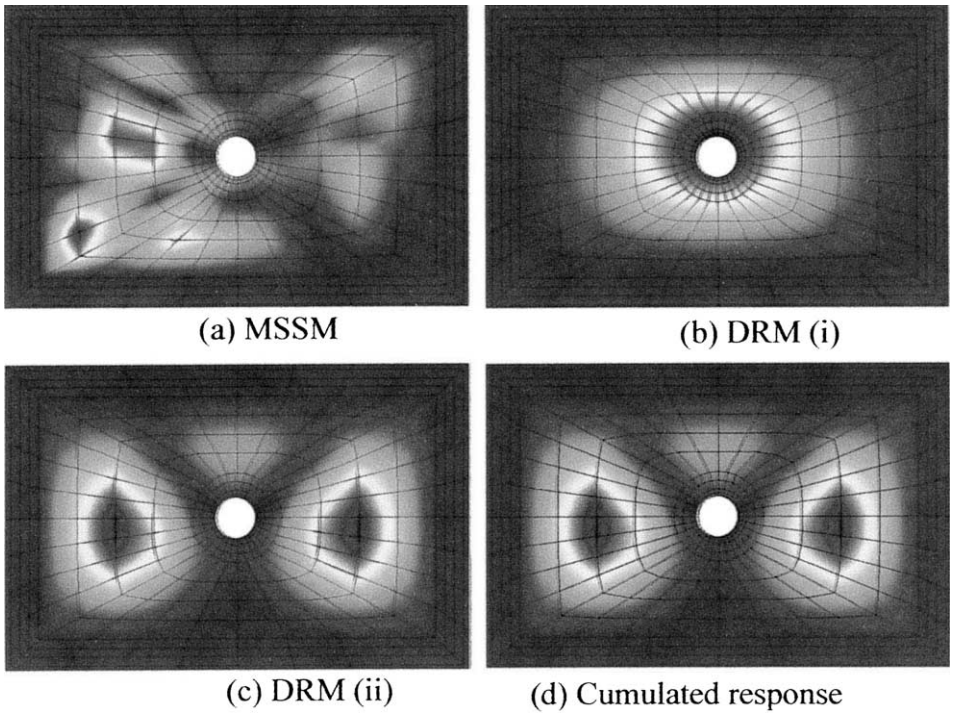

Fig. 6. Vibration amplitudes on the elementary cell obtained by different methods.

tion and the summation of some modes without weighting coefficients has no physical sense. This numerical result confirms the remark in Section 3.3: the use of MSSM is inappropriate for the present study and well beyond its intended use.

- For the DRM, the results are realistic and we are able to put forward two numerical areas for measure: (i) when the defect frequency is really weak (10 Hz), the results show that whatever the excitation point, the ideal measure area is the same and very close to the excitation point (Fig. 6b); (ii) when the defect frequency is greater than the first natural frequency (95 Hz), the calculation gives two other measure areas (Fig. 6c). In fact, the low frequency defects mainly excite the first mode of the frame; but the defects of higher frequencies provoke higher modes.
- The cumulated response (Fig. 6d) shows that the best measure zones fit with areas relative to the greatest defect frequency. This cumulation leads to a masking of the area corresponding to lower defect frequencies.

5. Defect detecting on a grinder

After the validation of these numerical tools, it seems interesting to study an industrial example. We create the CAD file of a grinder and import it in a FE code for numerical modeling (Fig. 7). The grinder is composed of two flasks in the two extremities, a protection steel sheet in the middle, four threaded stems of assembly, a stator, a rotor and two ball bearing SNR 6203 situated inside the two flasks.

5.1. Numerical determination of the sensor positions

The protection sheet is fixed on the flasks only by four screws and has no structural function. Moreover, it is experimentally proved that the measurement on this sheet is not reliable. So this sheet is not included in the numerical modeling (neither in the experiment). The two flasks are meshed with quadrangular and triangular shell elements, the stator is meshed with eight node hexahedral elements, the stator and stems are meshed with Timoshenko beam elements. Each ball bearing is modeled by four bearing elements. The whole system involves 19 190 degrees of freedom.

At first, the results of modal analysis are compared to the experimental ones for a flask with free–free boundary conditions. The relative errors are generally small, for the natural frequencies (Table 1), a mode shape comparison has confirmed this correlation with a little more errors. After this experimental vali-

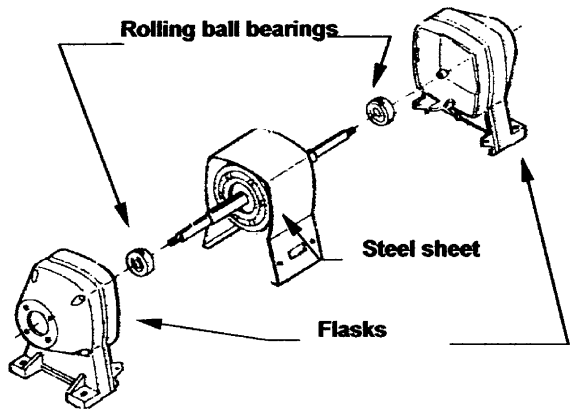

Fig. 7. Description of the grinder.

Table 1
Natural frequencies of a flask obtained numerically and experimentally

Mode	Experimental frequency (Hz)	EF frequency (Hz)	Relative error (%)
7	520	540	3.8
8	1010	1108	9.7
9	1263	1285	1.7
10	1601	1583	1.1
11	1660	1696	2.1
12	1745	1817	4.1
13	2000	1991	0.4

dation, the numerical procedure is used to obtain the sensitive areas to the defect excitations applied to the ball bearings of the grinder. For the ball bearing SNR 6203, the defect frequencies are: $f_{or} = 76.3$ Hz, $f_{ir} = 123.6$ Hz, $f_{ball} = 99.8$ Hz, $f_{cage} = 9.5$ Hz. Five nodes situated on the contour of the outer ring of the bearing are selected for the excitation force application (Fig. 8). At each node, the responses of the grinder are calculated for the excitation of four defect frequencies respectively.

The following comments can be given on the numerical results:

- Influence of the defect frequencies:

We note that these defect frequencies have a little influence on the calculated responses (Fig. 9a). The obtained sensor positions are good for all four defect excitations, since all defect frequencies are much smaller than the first natural frequency of the grinder, so they cannot excite other natural frequencies. This explains why the defect frequencies have a significant influence for the elementary cell but not for the grinder.

- Influence of excitation signal shapes:

The results show that the excitation signal shapes have a little influence on the calculation. Moreover, the pulse widths (10, 30 and 50% of the time period) have no effects on the results. It seems important to use a pulse signal instead of an harmonic one but the shape and width of the pulse is not essential for this kind of study.

- MSSM:

It is difficult to judge the quality of the results obtained with the MSSM because of the complexity of the structure, but the results are unusable (Fig. 9b). We note that the ideal measurement area is situated on the

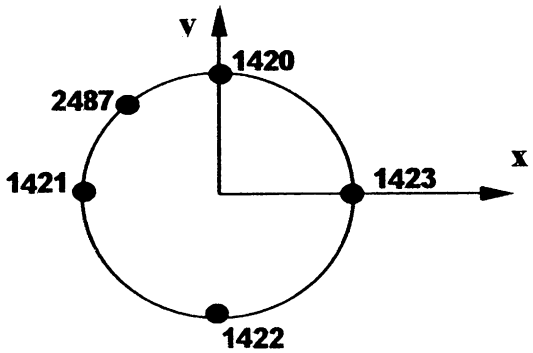

Fig. 8. Six nodes on the ball bearing for the excitation application.

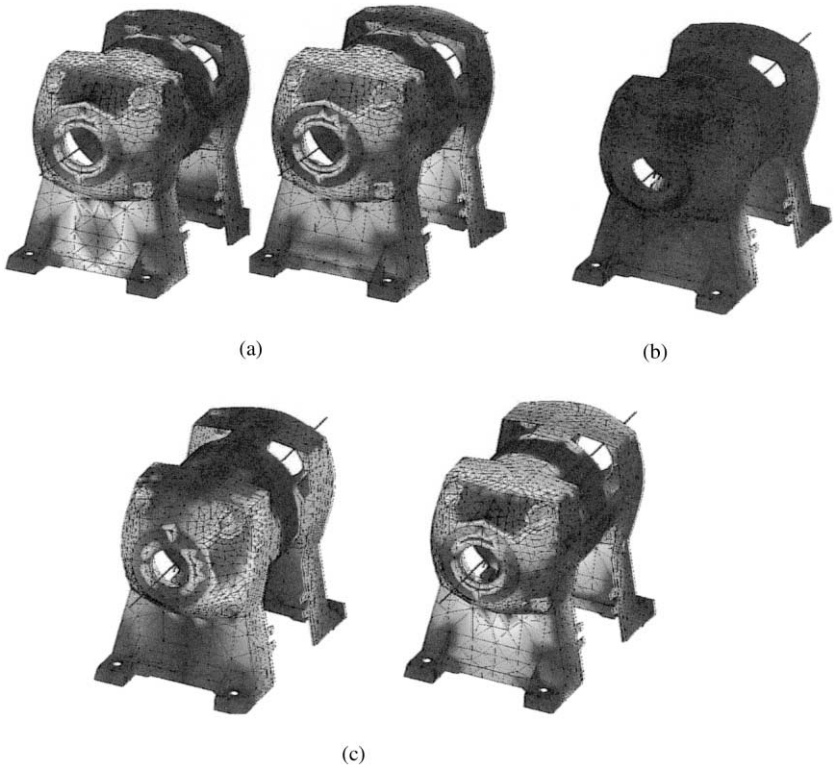

Fig. 9. Vibration amplitudes in normal directions obtained by different methods. (a) Influence of defect frequencies on spectral responses, (b) MSSM criteria, (c) ideal measurement area.

middle side of the grinder, just around fixation paths of the steel sheet. This part of the grinder is not easily accessible because of the steel sheet and screw fixations.

- DRM:

This method put forward two measurement areas: the top of the cone and the left top area of the grinder (Fig. 9c). The first one may be used when the bearing defect is situated at the node 1420 or 1422 (Fig. 8), the another one can be used for other defect positions. The results show that for most defect positions on the outer ring of the bearing the best sensor position is located on the left top of the grinder. The cone is not a good place, since it is difficult to set a sensor on it.

5.2. Experimental evidence

We have made an experimental device and a chipping defect on the outer ring of a bearing. The grinder works at normal speed. The objective is to compare the FRF at the optimum sensor zone (obtained numerically) with those at other places.

The envelope detection method (Carreau, 1999) allows to experimentally check (Appendix C) that the measured FRF in the numerical zone is more marked than the FRF at other places. Fig. 10 shows this difference between a node in the optimum zone (ref. NZ) and a node outside this zone (ref. OZ). We note that the maximal amplitude value at the node NZ is greater. This experimental validation confirms the previous numerical results.

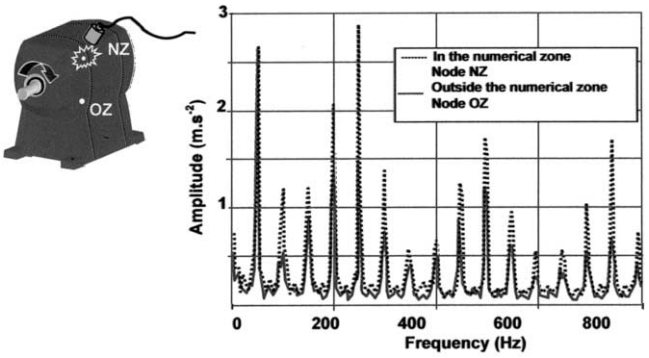

Fig. 10. Validation of the ideal numerical zone on the grinder.

This experiment shows that it is possible to use a numerical method in order to find an optimum measurement area on a revolving machine. This area can be used to monitor all chipping defects (on the inner ring, outer ring or balls of the bearings).

6. Conclusion

In this paper, a numerical methodology is proposed to determine optimum sensor positions for predictive maintenance. An analytical bearing model is adopted to avoid complicated computations. An explicit tangent stiffness matrix is obtained with the Newton–Raphson method. A bearing element is implemented into the commercial code ABAQUS. The non linear FE modeling allows to determine the tangent stiffness matrix at the given pre-load lever, then this matrix is used for the dynamic analysis. The defect excitations are assumed to be periodic such as the defects on the inner or external rings. The analysis of the response vectors in the frequency domain allows to find the most sensitive zones to the defect excitations.

An elementary unit shaft-ball bearing housing was modeled to study its spectral response to defect excitations. The comparison between the experimental and numerical results shows a good correlation. An industrial application was carried out and validated experimentally. This experiment shows that it is possible to choose, with a finite element modeling, an optimum measurement area on a revolving machine. This zone will be used to monitor chipping defects on a bearing of the grinder. This methodology gives more information to help engineers to design revolving machines with the point of view of predictive maintenance.

Appendix A. Formulas to determine the main defect frequencies of a rolling ball (or roller) bearing

Outer ring frequency	Inner ring frequency	Cage frequency	Ball frequency
$f_{or} = \frac{f_{rot} \times N_b}{2}\left(1 - \frac{d}{D}\cos\alpha\right)$	$f_{ir} = \frac{f_{rot} \times N_b}{2}\left(1 + \frac{d}{D}\cos\alpha\right)$	$f_{cage} = \frac{f_{rot}}{2}\left(1 - \frac{d}{D}\cos\alpha\right)$	$f_{ball} = \frac{f_{rot}}{2} \times \frac{D}{d}\left[1 - \left(\frac{d\cos\alpha}{D}\right)^2\right]$

With:

- N_b: the number of rolling element,
- D: the primitive diameter,
- D: the rolling element diameter,

- α: the contact angle,
- f_{rot}: the frequency rotation of the inner ring (the outer one is supposed fix).

Appendix B. Fourier's coefficients for pulse shape

Pulse shape	F_0	F_n
Rectangular	$A\frac{\Delta T}{T}$	$\frac{2A}{\pi k}\sin(\pi k\frac{\Delta T}{T})$
Triangular	$\frac{A}{2}\frac{\Delta T}{T}$	$\frac{2A}{\pi^2 k^2\frac{\Delta T}{T}}(1-\cos(\pi k\frac{\Delta T}{T}))$
Half sine	$\frac{2A}{\pi}\frac{\Delta T}{T}$	$\frac{4A}{\pi(1-4k^2(\frac{\Delta T}{T})^2)}\frac{\Delta T}{T}\cos(\pi k\frac{\Delta T}{T})$

With:

- A: the excitation force amplitude,
- ΔT: defect time width on a period,
- T: the defect excitation period.

Appendix C. Envelope detection or high frequency resonance technique

This method is used to detect precocious defect. With the high resonance frequencies of the frame ($\approx$10 kHz), the envelope detection permit to determine the defects generated by shocks in low frequency range ($<$1 kHz).

The procedure is:

- Determination of the frame frequencies (0–10 kHz).
- Determination of the time signal.

- Fourier transform signal + filtering around the chosen resonance in a range enclosing defect frequencies and harmonics.

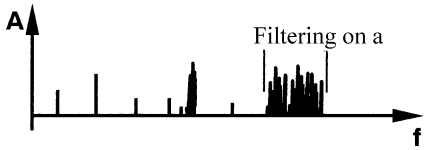

- Inverse Fourier transform of the filter spectrum. The result is then a time signal clearer, which allows to show the shocks and signal periodicity.

- The high frequencies parts are suppressed and the envelope detection is realized with the Hilbert transform followed by a straightening.

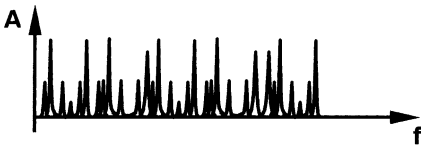

- Then, the Fourier transform is done on this signal and frequencies thus obtained are precisely those which are wanted.

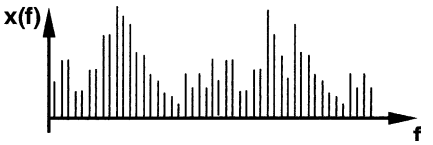

By doing the Fourier transform on the log of this spectrum and by squaring the result, we obtain a frequency representation where we find only the wanted fundamental frequencies.

References

AFNOR, 1995. Surveillance des machines par analyse des vibrations. ISBN: 2123090123.

Bogard, F., 2000. Développement d'une approche numérique visant à optimiser le suivi vibratoire des constituants d'une machine tournante. Thèse de l'Université de Reims.

Carreau, D., 1999. Analyse des vibrations pour la surveillance des roulements. Maintenance et Entreprise, no. 436.

De Clerck, J.P., Avitabile, P., 1996. Development of several new tools for pre-test evaluation. IMAC 14.

Demul, J.M., Vree, J.M., Maas, D.A., 1989. Equilibrium and associated load distribution in ball and roller bearings loaded in 5 degrees of freedom while neglecting frictions. Part I: General theory and application to ball bearings. Transactions of the ASME, Journal of Tribology 111, 142–148.

Harris, T.A., 1991. Rolling Bearings Analysis, third ed. Lavoisier.

Jones, A.B., 1960. A general theory for elastically constrained ball and radial roller bearings under arbitrary loud and speed conditions. Journal of Basic Engineering 82, 309–320.

Kraus, J., Blech, J.J., Braum, S.G., 1987. In situ determination of roller bearing stiffness and damping by modal analysis. Journal of vibration acoustics stress and reliability in design 109, 235–240.

Lim, T.C., Singh, R., 1990. Vibration transmission through rolling element bearings. Part I: bearings stiffness formulation. Journal of Sound and Vibration 139, 179–199.

Max, J., 1987. Méthode et techniques de traitement du signal et applications aux mesures physiques. Ed Masson, ISBN: 222580785x.

Morel, J., 1992. Vibrations des machines et diagnostic de leur état mécanique. In: Eyrolles (Ed.), ISSN: 03994198.

Palmgren, A., 1959. Ball and Roller Bearing Engineering, third ed. S. Burkank & Co, Philadelphia.

Structural Dynamics Toolbox, 1999. Version 4.0.

Tandon, N., Choudury, A., 1997. An analytical model for the prediction of the vibration response of rolling element bearings due to a localized defect. Journal of Sound and Vibrations 205 (3), 275–292.